Plasmonic particles set into fast orbital motion by an optical vortex beam WARI SC, 1992, JOURNAL OF MODERN OPTICS, V39, P1097

Plasmonic particles set into fast orbital motion by an optical vortex beam

Anni Lehmuskero,[1,*] Yanming Li,[2] Peter Johansson,[1,3] and Mikael Käll[1,4]

[1]*Department of Applied Physics, Chalmers University of Technology, Gothenburg, 412 96, Sweden*
[2]*Electrical & Computer Engineering Department, NC State University, Raleigh, North Carolina 276 95, USA*
[3]*School of Science and Technology, Örebro University, Örebro, 701 82, Sweden*
[4]*mikael.kall@chalmers.se*
[*]*anni.lehmuskero@chalmers.se*

Abstract: We optically trap plasmonic gold particles in two dimensions and set them into circular motion around the optical axis using a helically phased vortex laser beam. The orbiting frequency of the particles reaches 86 Hz, which corresponds to a particle velocity of the order 1 mm per second, for an incident laser power of a few tens of milliwatts. The experimentally determined orbiting frequencies are found to be well in line with the notion that the beam carries an orbital angular momentum of $\hbar l$ per photon.

OCIS codes: (140.7010) Laser trapping; (080.4865) Optical vortices; (350.4855) Optical tweezers or optical manipulation; (240.6680) Surface plasmons.

References and Links

1. A. M. Yao and M. J. Padgett, "Orbital angular momentum: origins, behavior and applications," Adv. Opt. Photonics **3**(2), 161–204 (2011).
2. N. B. Simpson, K. Dholakia, L. Allen, and M. J. Padgett, "Mechanical equivalence of spin and orbital angular momentum of light: an optical spanner," Opt. Lett. **22**(1), 52–54 (1997).
3. H. He, M. E. J. Friese, N. R. Heckenberg, and H. Rubinsztein-Dunlop, "Direct observation of transfer of angular momentum to absorptive particles from a laser beam with a phase singularity," Phys. Rev. Lett. **75**(5), 826–829 (1995).
4. M. Dienerowitz, M. Mazilu, P. J. Reece, T. F. Krauss, and K. Dholakia, "Optical vortex trap for resonant confinement of metal nanoparticles," Opt. Express **16**(7), 4991–4999 (2008).
5. K. Ladavac and D. G. Grier, "Microoptomechanical pumps assembled and driven by holographic optical vortex arrays," Opt. Express **12**(6), 1144–1149 (2004).
6. T. Kolb and G. Whyte, "Rotation of optically trapped living cells for single-cell tomography," in *Optics in the Life Sciences Conference,* 2013 OSA Technical Digest Series (Optical Society of America, 2013), paper TM4D.4.
7. L. Paterson, M. P. MacDonald, J. Arlt, W. Sibbett, P. E. Bryant, and K. Dholakia, "Controlled rotation of optically trapped microscopic particles," Science **292**(5518), 912–914 (2001).
8. Y. Arita, A. W. McKinley, M. Mazilu, H. Rubinsztein-Dunlop, and K. Dholakia, "Picoliter rheology of gaseous media using a rotating optically trapped birefringent microparticle," Anal. Chem. **83**(23), 8855–8858 (2011).
9. A. I. Bishop, T. A. Nieminen, N. R. Heckenberg, and H. Rubinsztein-Dunlop, "Optical microrheology using rotating laser-trapped particles," Phys. Rev. Lett. **92**(19), 198104 (2004).
10. J. Leach, H. Mushfique, R. di Leonardo, M. Padgett, and J. Cooper, "An optically driven pump for microfluidics," Lab Chip **6**(6), 735–739 (2006).
11. M. E. J. Friese, H. Rubinsztein-Dunlop, J. Gold, P. Hagberg, and D. Hanstorp, "Optically driven micromachine elements," Appl. Phys. Lett. **78**(4), 547–549 (2001).
12. P. Galajda and P. Ormos, "Complex micromachines produced and driven by light," Appl. Phys. Lett. **78**(2), 249–251 (2001).
13. L. Tong, V. D. Miljković, and M. Käll, "Alignment, rotation, and spinning of single plasmonic nanoparticles and nanowires using polarization dependent optical forces," Nano Lett. **10**(1), 268–273 (2010).
14. A. Lehmuskero, R. Ogier, T. Gschneidtner, P. Johansson, and M. Käll, "Ultrafast spinning of gold nanoparticles in water using circularly polarized light," Nano Lett. **13**(7), 3129–3134 (2013).
15. V. Garcés-Chávez, K. Volke-Sepulveda, S. Chávez-Cerda, W. Sibbett, and K. Dholakia, "Transfer of orbital angular momentum to an optically trapped low-index particle," Phys. Rev. A **66**(6), 063402 (2002).
16. V. Garcés-Chávez, D. McGloin, M. J. Padgett, W. Dultz, H. Schmitzer, and K. Dholakia, "Observation of the transfer of the local angular momentum density of a multiringed light beam to an optically trapped particle," Phys. Rev. Lett. **91**(9), 093602 (2003).

#203613 - $15.00 USD Received 26 Dec 2013; revised 10 Feb 2014; accepted 10 Feb 2014; published 18 Feb 2014

17. K. Volke-Sepulveda, V. Garcés-Chávez, S. Chávez-Cerda, J. Arlt, and K. Dholakia, "Orbital angular momentum of a high-order Bessel light beam," J. Opt. B Quantum Semiclassical Opt. **4**(2), S82–S89 (2002).
18. A. T. O'Neil, I. MacVicar, L. Allen, and M. J. Padgett, "Intrinsic and extrinsic nature of the orbital angular momentum of a light beam," Phys. Rev. Lett. **88**(5), 053601 (2002).
19. Y. Zhao, J. S. Edgar, G. D. M. Jeffries, D. McGloin, and D. T. Chiu, "Spin-to-orbital angular momentum conversion in a strongly focused optical beam," Phys. Rev. Lett. **99**(7), 073901 (2007).
20. K. Ladavac and D. G. Grier, "Colloidal hydrodynamic coupling in concentric optical vortices," Europhys. Lett. **70**(4), 548–554 (2005).
21. Y. Li, J. Kim, and M. J. Escuti, "Controlling orbital angular momentum using forked polarization gratings," Proc. SPIE **7789**, 77890F (2010).
22. S. C. Tiwari, "Geometrical phase in optics; quantal or classical?" J. Mod. Opt. **39**, 1097–1105 (1992).
23. M. V. Berry, "The adiabatic phase and Pancharatnam's phase for polarized light," J. Mod. Opt. **34**(11), 1401–1407 (1987).
24. J. E. Curtis and D. G. Grier, "Structure of optical vortices," Phys. Rev. Lett. **90**(13), 133901 (2003).
25. A. O. Govorov and H. H. Richardson, "Generating heat with metal nanoparticles," Nano Today **2**(1), 30–38 (2007).
26. R. L. Fogel'son and E. R. Likhachev, "Temperature dependence of viscosity," Tech. Phys. **46**(8), 1056–1059 (2001).
27. P. V. Ruijgrok, N. R. Verhart, P. Zijlstra, A. L. Tchebotareva, and M. Orrit, "Brownian fluctuations and heating of an optically aligned gold nanorod," Phys. Rev. Lett. **107**(3), 037401 (2011).
28. D. Rings, R. Schachoff, M. Selmke, F. Cichos, and K. Kroy, "Hot Brownian motion," Phys. Rev. Lett. **105**(9), 090604 (2010).
29. J. Happel and H. Brenner, *Low Reynolds Number Hydrodynamics* (Kluwer, 1991).
30. M. J. Padgett, "On diffraction within a dielectric medium as an example of the Minkowski formulation of optical momentum," Opt. Express **16**(25), 20864–20868 (2008).
31. I. Brevik, "Experiments in phenomenological electrodynamics and the electromagnetic energy-momentum tensor," Phys. Rep. **52**(3), 133–201 (1979).
32. Y. Arita, M. Mazilu, and K. Dholakia, "Laser-induced rotation and cooling of a trapped microgyroscope in vacuum," Nat. Commun. **4**, 2374 (2013).

1. Introduction

The property that light in certain cases carries orbital and spin angular momentum can be utilized to set microscopic objects into rotational motion. Each photon of circularly polarized light carries a spin angular momentum (SAM) of $\pm\hbar$. The SAM can be transferred to an illuminated object if the photon is absorbed or forced to change its polarization state, for example through interaction with a birefringent object. Orbital angular momentum (OAM), on the other hand, originates from the spatial phase distribution properties of a light field. A laser beam that carries OAM, a so-called optical vortex beam, is typically described by higher order Laguerre-Gaussian (LG) modes [1]. The OAM results from a phase component of the form $\exp(i l\phi)$, where the mode index l defines the magnitude of the OAM as $\hbar l$ per photon, which generates a linear photon momentum component in the azimuthal direction around the optical axis of the beam. This component can force objects to spin similarly to circularly polarized light if the particle is *large* compared to the beam diameter [2,3].

Laser tweezers based on a tightly focused laser beam is a delicate and accurate tool to trap and manipulate microscopic objects using the optical gradient force. Ordinary laser tweezers pull an object to the focus of a Gaussian intensity distribution, where the object can be rotated due to SAM transfer. However, a focused vortex beam has an annular focal intensity distribution, which implies that an object that is *small* compared to the beam focus tend to orbit the dark center of the beam due to OAM transfer from scattered and absorbed photons [4,5]. The effect of OAM transfer is thus qualitatively different from SAM transfer in this case, that is, a small object tend to spin in a circular orbit rather than around its own axis.

Optically induced rotation by laser tweezers has been investigated in the context of cell biology, to manipulate living cells and chromosomes [6,7]; microrheology [8,9]; microfluidics, as micro-optomechanical pumps [5,10]; and micromechanics [11,12]. All these applications rely on a significant rotational motion and may therefore benefit from faster rotation speeds and more efficient angular momentum transfer.

#203613 - $15.00 USD Received 26 Dec 2013; revised 10 Feb 2014; accepted 10 Feb 2014; published 18 Feb 2014

We have previously investigated how SAM transfer can be used to set plasmonic nanostructures into rotational motion [13]. Recently, we demonstrated that round colloidal gold particles with an average radius of R = 200 nm can reach spinning frequencies in the kHz range in water if subject to a focused beam of circularly polarized laser light with a power of the order of a few tens of mW [14]. These particles have three properties that contribute to make fast rotation possible. First, they have large absorption cross-sections, resulting in an efficient transfer of SAM from the incident photons to the particles. Secondly, they heat up, which somewhat surprisingly appears as a positive contribution to the spinning frequency by lowering the viscosity, and thereby the drag force, of the surrounding water. Thirdly, they are highly polarizable, resulting in a large gradient force and, therefore, a more stable trap. As we will show in this contribution, the *orbital rotation frequency* of a trapped object due to OAM transfer can also be increased substantially by exploiting these very special optical properties of plasmonic nanoparticles. To the best of our knowledge, orbital rotation frequencies reported to date have been of the order of ~1 Hz for laser powers in the range 10 mW to 1 W [4,5,15–20], with a record value of ~6.5 Hz obtained for an incident laser power of ~520 mW reported by Garcés-Cháves et al. [16]. The highest value found in the present study was 86 Hz for 73 mW of incident laser power, that is, one to two orders of magnitudes higher than previous literature data. This finding may have significant impact on a variety of application areas that involve nanooptics and nanofluidics.

2. Optically induced rotation with a *q*-plate

A schematic illustration of the experimental setup is shown in Fig. 1(a). We focus laser light with a wavelength of 830 nm into the volume between two cover-glass slides where the sample is located. The sample is an aqueous colloid droplet containing the same type of gold nanoparticles as investigated in Ref [14]. The radiation pressure of the laser beam pushes the particles close to the cover glass, resulting in an essentially two-dimensional trapping configuration. A dark-field condenser is used to illuminate the particles. The orbital rotation frequency is determined from the scattered intensity through an autocorrelation of the photon count rate obtained from a specific point on the particle orbit and/or by analyzing a video recording.

The optical vortex is generated using a so-called *q*-plate that produces a helical wave front. The *q*-plate is a birefringent thin film formed by a liquid crystal polymer with an optical axis that varies spatially as $\Phi = q\phi + \Phi_0$ where q is the topological charge and ϕ is the azimuthal angle in polar coordinates. Figure 1(b) illustrates the structure of the *q*-plate by imaging it positioned between two crossed polarizers. The details of the fabrication can be found in Ref [21]. The *q*-plate manipulates the phase of an incident plane wave [22,23] in such a way that a smooth helical phase front with mode index $l = \pm 2q$ is produced. The thickness of the *q*-plate was designed such that it causes a phase retardation of $\lambda/2$ at the 830 nm trapping wavelength and a pure helical mode for circularly polarized incident light. The size of the LG annular ring is dependent on the mode number [24]. We chose l = 8, which gives a beam radius distinctly larger than the particle diameter for the 100x, NA≈1.2 optics used to focus the laser beam in the sample plane. As a result, a trapped particle will follow a circular orbit with a radius of approximately 2 μm, as indicated in Fig. 1(c). By using a *q*-plate to create the optical vortex, we expect to obtain a uniform intensity distribution and avoid the discontinuities often encountered when using spatial light modulators [24] or computer generated holograms [17]. In addition, the trap is further stabilized by using an optical vortex beam that is circularly polarized, which yields optical gradient forces that exhibit circular symmetry in the radial direction around the optical axis. This is unlike linear polarization for which the asymmetry of the light scattering pattern causes an uneven confinement of the particle along the high intensity ring (shown in Section 6).

#203613 - $15.00 USD Received 26 Dec 2013; revised 10 Feb 2014; accepted 10 Feb 2014; published 18 Feb 2014

3. Theoretical torques and orbiting frequencies

The gradient force confines a trapped particle to the high intensity region of the annular LG beam, where it is set in orbital motion at a certain constant speed for a given incident laser power. In a first approximation, the speed is determined by two counterbalancing torques in

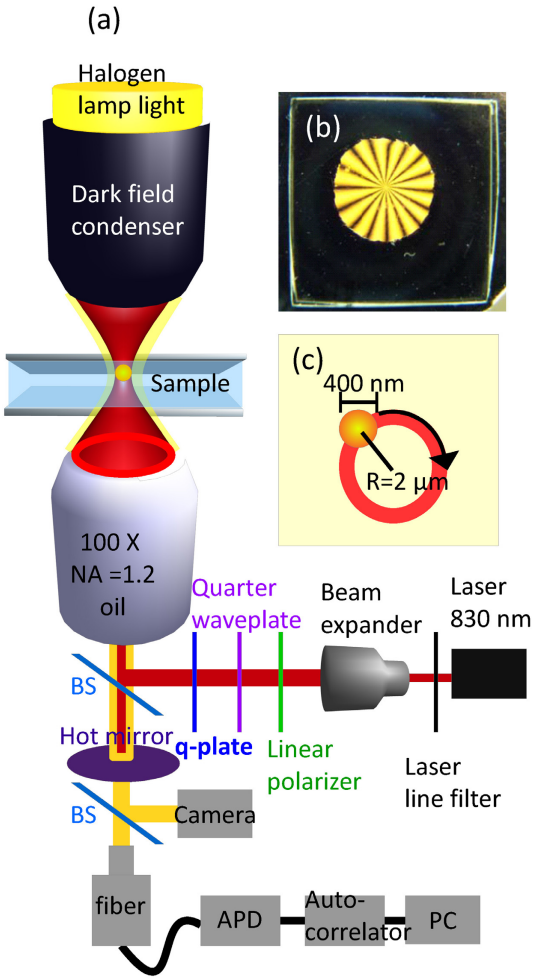

Fig. 1. **(a)** Illustration of trapping and detection of orbiting nanoparticles. The 830 nm laser beam is expanded to fill the back aperture of the microscope objective, polarized and focused on the sample through the *q*-plate. Most of the back-scattered laser light is filtered away by the hot mirror but a small fraction reaches the APD and can be analyzed with the autocorrelator. **(b)** An image of the *q*-plate used to generate the optical vortex beam when it is positioned between two crossed polarizers. **(c)** The optically trapped particle moves along a circular orbit of radius ~2 μm, as determined by the optical vortex beam intensity profile.

the optical trap; the optical torque and the viscous drag torque. The former is dependent on the intensity I, the particle absorption cross section $\sigma_{a,}$ the particle transport cross section $\beta\sigma_s$ (where σ_s is the ordinary scattering cross section), the mode number l, and the angular frequency of the incident light ω_0 according to

$$\tau_o = (\sigma_a + \beta\sigma_s) Il / \omega_0. \quad (1)$$

#203613 - $15.00 USD Received 26 Dec 2013; revised 10 Feb 2014; accepted 10 Feb 2014; published 18 Feb 2014

The transport cross section $\beta\sigma_s$ determines the actual contribution of the scattered photons to the momentum transfer. It can be expressed in terms of the differential scattering cross section $d\sigma_s/d\Omega$ by an integration over all scattering directions (θ,φ)

$$\beta\sigma_s = \int \frac{d\sigma_s}{d\Omega}(1-\cos\theta)\sin\theta d\theta d\varphi, \tag{2}$$

where θ is the scattering angle. Using Mie theory, we find $\beta = 0.63$ for a 200 nm gold sphere in water illuminated by light with a vacuum wavelength of 830 nm. We note in passing that the scattering cross-section does not contribute to the spinning of particles caused by SAM transfer investigated in [14].

The drag torque on a particle in orbiting motion in a viscous medium can be derived from the Stokes equation assuming a low Reynolds number [15]. The result is

$$\tau_v = -6\pi\eta r^2 R_0\omega, \tag{3}$$

where η is the dynamic viscosity of the surrounding medium, r is the radius of the orbit, R_0 the radius of the particle, and ω is the orbiting angular frequency. When the torques balance each other, $\tau_o + \tau_v = 0$, we obtain a constant orbiting frequency

$$\omega = \frac{(\sigma_a+\beta\sigma_s)Il}{6\pi\eta r^2 R_0\omega_0}. \tag{4}$$

Note, that by increasing the mode number l we would get lower orbiting frequency because of the increase in the beam radius [24] and the consequent drop in the intensity.

The viscosity depends on the water temperature. At the particle surface, and assuming steady-state heat transport, the excess temperature is $\Delta T = (\sigma_a I)/(4\pi R_0\kappa)$ where $\kappa = 0.58$ W/Km is the heat conductivity of water [25]. The viscosity of water at temperature T can then be estimated from [26]

$$\eta(T) = \eta_0 \exp\left[\frac{E_a}{N_A k_B (T-T^*)}\right], \tag{5}$$

where $\eta_0 = 24.2$ μPa·s, $E_a = 4.74$ kJ/mol is an activation energy, k_B is Boltzmann's constants, N_A is Avogadro's number and $T^* = 140$K is a temperature offset. Since the particle is in translational motion, both the particle surface temperature and the surrounding bath temperature have an effect on the viscosity experienced by the particle. In this case a fairly accurate value for the viscosity can be found by using an effective temperature T_{eff} in the expression for η. Here we have used the effective temperature [27,28]

$$T_{eff} = (T_{bath} + T_p)/2. \tag{6}$$

4. Autocorrelation function analysis

The rotation frequency was obtained from the autocorrelation signal of the scattered photon count rate which exhibits a periodicity that is determined by the average rotational motion of the particle. Random thermal forces (Brownian motion) lead to fluctuations in the particle velocity and, as a consequence, to a decay of the autocorrelation amplitude [14]. Two examples of the autocorrelation signal are given in Fig. 2 together with dark field images of the trapped particle taken with a camera with an integration time of 41.7 ms. As can be seen in Fig. 2(c), the particle travels about half of the orbital circumference in the case when the laser power is 13.3 mW. This corresponds to an autocorrelation signal periodicity of 70.3 ms, see Fig. 2(a) (14 Hz, the green-blue line with circular marks in Fig. 3). At the highest laser power, 73.1 mW, the period is reduced to 11.6 ms, see Fig. 2(b) (86 Hz, the red line with diamond marks in Fig. 3), and it is then no longer possible to distinguish the distance traveled by the particle, see Fig. 2(d) (Media 1).

#203613 - $15.00 USD Received 26 Dec 2013; revised 10 Feb 2014; accepted 10 Feb 2014; published 18 Feb 2014

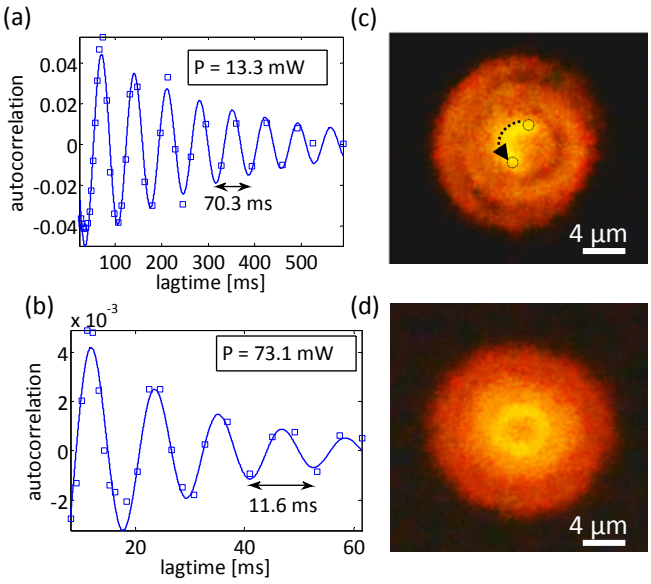

Fig. 2. **(a)** Autocorrelation functions of the photon count rate for a laser power of 13.3 mW and **(b)** 73.1 mW, corresponding to the circular and diamond data points in Fig. 3, respectively. **(c)** Image of an orbiting particle for a laser power of 13.3 mW. The dashed line indicates the movement of the particle during the integration time of the camera (41.7 ms) **(d)** Image for the case of a laser power of 73.1 mW (Media 1). The concentric rings and diffuse scattering in (c) and (d) are mainly an image artifact caused by a slight displacement of the particle relative to the focal plane along the optical axis.

5. Experimental orbiting frequencies

Figure 3 shows the theoretical orbiting frequency ($f = \omega/2\pi$) as a function of laser power together with the measured frequencies for five different particles. The theoretical values were obtained from Eqs. (4)–(6) using theoretical absorption and scattering cross sections, σ_a and σ_s, obtained from Mie theory [14]. The intensity profile of the beam in the focal plane was approximated as a homogenous ring with a width equal to the wavelength of light [24]. As illustrated in the inset of Fig. 3, an increasing laser power leads to a rise in the particle surface temperature, and, consequently, a decrease in water viscosity [14]. This in turn promotes a higher rotation frequency, i.e. causing the upturn in the theoretical curve for higher laser powers.

Although the five different particles exhibit a significant spread in orbiting frequencies for the same laser power, a feature that is most probably due to small differences in optical properties and morphologies of the individual particles, the overall power dependence is similar. An unexpected feature of the experimental curves that is difficult to explain is that they seem to extrapolate to a finite orbital frequency at zero laser power. This may indicate that saturation effects not accounted for in the theoretical analysis are at play for the investigated power range. There can be a number of possible causes to this discrepancy. For example, the theory assumes that a particle is completely surrounded by water while in reality it is pushed against the glass surface by the power dependent radiation pressure. If the particle comes closer to the cover glass with increasing laser power, one expects an effectively increasing viscous friction [29]. It can also be expected that the thermal balance and the precise intensity distribution is sensitive to the exact position of the trapped particle relative to the confining glass surface and the focal position. Unfortunately, it was not possible to extend the rotation experiments to lower laser powers because the Brownian motion of the particles then overcome the optical gradient force and the particles escape from the trap. Nevertheless,

#203613 - $15.00 USD Received 26 Dec 2013; revised 10 Feb 2014; accepted 10 Feb 2014; published 18 Feb 2014

given the simplifying theoretical assumptions, we find the agreement between the theoretical and experimental rotation frequencies to be surprisingly good. The highest experimental orbiting frequency we observe, 86 Hz, corresponds to a particle velocity of 1.1 mm / s. Using Eq. (3), we can roughly estimate the torque and the angular force acting on a particle (assuming that the viscous drag force is the only frictional force). The corresponding values are in order of nN·nm and pN, respectively, where the force is obtained by dividing the torque with the orbital radius.

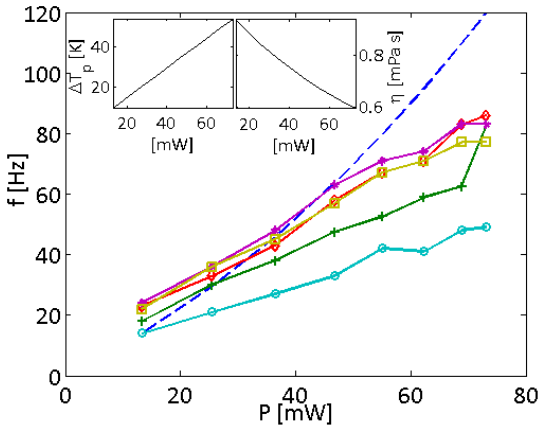

Fig. 3. Theoretical (dashed line) and experimental orbital rotation frequencies for five different particles as a function of the sample-plane laser power. The left-hand inset shows an estimate of the temperature rise on the particle surface obtained from the heat transport equation while the right-hand inset shows the corresponding temperature dependent viscosity relevant to translational particle motion.

6. Force calculations from electrodynamics simulations

We also made a more detailed calculation of the optical forces acting on a gold particle in a LG beam. To this end, we projected the fields of a LG beam onto the vector spherical harmonics describing the electromagnetic field around a sphere, and evaluated the optical force on the particle by employing the Minkowski stress tensor [30,31]. Figure 4 shows the distribution of radial and angular optical forces on a gold particle of radius 200 nm in an (ideal) LG beam with l = 8 and a beam waist of 1 μm for both circularly and linearly polarized light. The laser power is 20 mW. The resulting force distributions are, as stated above, circularly symmetric for circularly polarized light, whereas for linear polarization the distribution is uneven. The magnitudes of the forces are consistent with the notion that, in a medium of refractive index n, a photon carries linear momentum $n\hbar\omega/c$. In case of OAM, the increase of photon momentum in an optically dense medium is offset by an effective decrease of the radius vector, and, just as in vacuum, a photon in a LG beam with mode number l carries angular momentum $\hbar l$. Also this fact is accurately reproduced by the numerical results found here, thus justifying the expressions we have used for the optical torque above.

7. Conclusions

In conclusion, we have demonstrated that subwavelength plasmonic gold particles illuminated by a Laguerre-Gaussian beam with a certain mode number l can be set to rotate fast along a circular orbit. We determined the rotational speed and frequency of the particle along the orbit by measuring the autocorrelation function of the scattered light intensity. A simple but still fairly accurate estimate of the viscous forces acting on the particle shows that the measured rotational frequencies are consistent with the notion that each photon carries orbital angular momentum $\hbar l$ that is transferred entirely to the particle upon absorption and partially,

#203613 - $15.00 USD Received 26 Dec 2013; revised 10 Feb 2014; accepted 10 Feb 2014; published 18 Feb 2014

depending on the scattering angle, upon scattering. In terms of applications, the experiments indicate that plasmonic particles could be utilized for micromechanics, microfluidics and other types of micromanipulation systems where the high orbital rotation rate is of importance. An interesting question open to further investigation is the possible interplay between the orbital rotational motion of the particle and the rotation around the particles own axis caused by absorption of circularly polarized light [19,32].

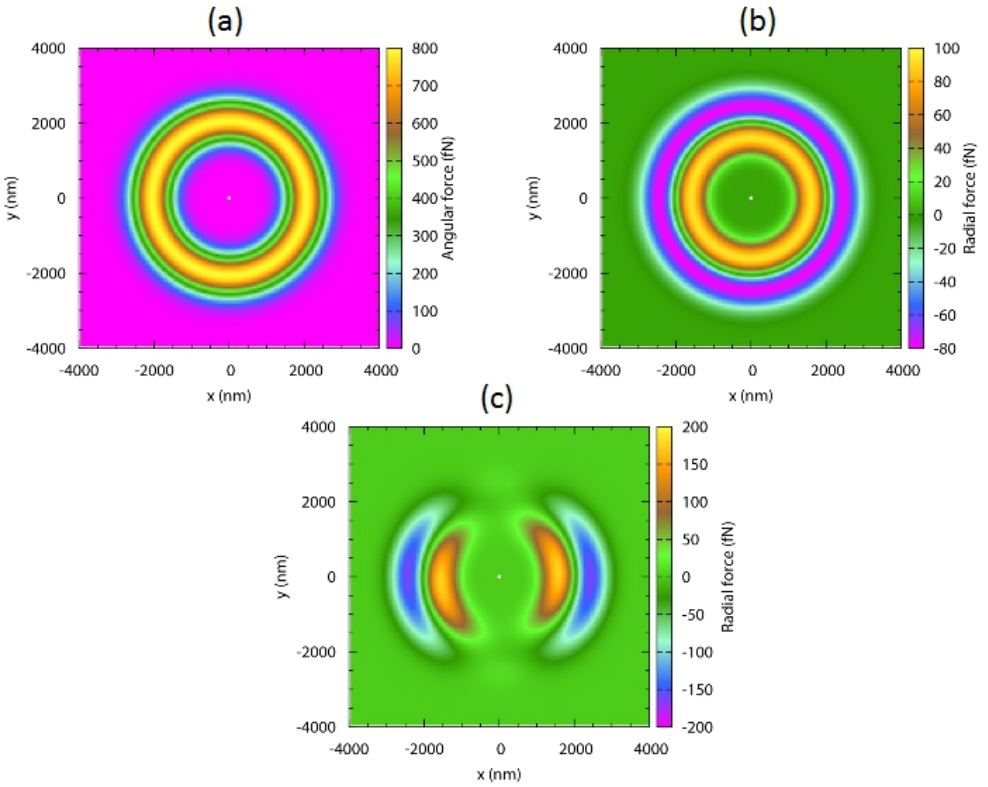

Fig. 4. **(a)** The angular force on a spherical gold particle of radius 200 nm in water illuminated by a LG beam of vacuum wavelength 830 nm, mode number $l = 8$, a beam waist of 1 μm, and a total power of 20 mW. This force pattern can drive the particle along a circular pattern. **(b)** The in-plane radial force in the same situation for circularly polarized light. The radial force confines the particle to moving within the ring of high light intensity, hence stabilizing the circular motion driven by the angular forces. **(c)** For light polarized linearly (along the x-axis), the radial force varies substantially along the high intensity ring.

Acknowledgments

We would like to thank the Göran Gustafsson Foundation, the Swedish Research Council, and the Chalmers Nanoscience Area of Advance for their financial support. AL and YL gratefully acknowledge the support of the Emil Aaltonen Foundation and the National Science Foundation (NSF grant ECCS-0955127), respectively. In addition, YL would like to thank Dr. Michael J. Escuti for the helpful discussions.